

Proton conductive polyoxoniobate frameworks constructed from nanoscale $\{\text{Nb}_{68}\text{O}_{200}\}$ cages

Yu-Diao Lin,^a Zeng-Kui Zhu,^a Rui Ge^a, Hao Yu,^a Zhong Li,^a Cai Sun,^a Yan-Qiong Sun,^a Xin-Xiong Li^{*ab} and Shou-Tian Zheng^{*a}

^a State Key Laboratory of Photocatalysis on Energy and Environment, College of Chemistry, Fuzhou University, Fuzhou, Fujian 350108, China.

^b State Key Laboratory of Structural Chemistry, Fujian Institute of Research on the Structure of Matter, Chinese Academy of Sciences, Fuzhou, Fujian 350002, China.

This file includes:

Section S1: Experiment and Methods

Section S2: Additional Tables

Section S3: Additional Figures and Characterizations

Section S4: References

Section S1: Experiment and Methods

1. Materials and General methods:

All chemical materials were commercially purchased without further purification. Elemental analyses of C, H, N, S and O were conducted by a Vario EL cube elemental analyzer. Infrared (IR) spectra (KBr pellet) were performed on an Opus Vetex 70 FT-IR infrared spectrophotometer in the range of 400-4000 cm^{-1} . Powder X-ray diffraction (PXRD) patterns were recorded on a Rigaku DMAX 2500 diffractometer with $\text{CuK}\alpha$ radiation ($\lambda=1.54056\text{\AA}$). Thermogravimetric analyses were conducted using a Mettler Toledo TGA/SDTA 851^e analyzer in an N_2 -flow atmosphere with a heating rate of 10 $^\circ\text{C}/\text{min}$ at a temperature of 25-800 $^\circ\text{C}$. The UV-vis spectra were measured on a SHIMADZU UV-2600 UV-visible spectrophotometer. Simulated XRD data were simulated by the Mercury Software with the step of 0.02 $^\circ$ from 5 $^\circ$ to 50 $^\circ$ ($\lambda=1.54056\text{\AA}$).

2. Synthesis

Synthesis of 1: A mixture of solid $\text{K}_7\text{HNb}_6\text{O}_{19}\cdot 13\text{H}_2\text{O}$ (0.275g, 0.2 mmol), $\text{CuCl}_2\cdot 2\text{H}_2\text{O}$ (0.100 g, 0.588 mmol), $\text{K}_2\text{B}_4\text{O}_7\cdot 4\text{H}_2\text{O}$ (0.100 g, 0.327 mmol), $\text{Sn}(\text{CH}_3)_2\text{Cl}_2$ (0.200 g, 0.910 mmol), 0.2ml en and 80ul 1H-1,2,3-Triazole were dissolved in 8ml deionized water. After being stirred in a 20ml vial for an hour, the resulting mixture was heated at 100 $^\circ\text{C}$ for 3 days and was cooled to room temperature. Then the resulting mixture stood for another 12 hours, and cubic crystals were finally obtained. Yield: 16.21% (based on Nb). The pH values before and after the reaction are 7.9 and 8.1, respectively.

Synthesis of 2: 2 was prepared by a procedure similar to that of 1, except for the replacement of 1H-1,2,3-triazole for pyrrole (0.080 g, 1.16 mmol). Yield: 18 % (based on Nb). The pH values before and after the reaction are 8.1 and 8.5, respectively.

3. Synthesis Discussion

In the synthesis process, there are four key factors contributing to our compounds. (1) We tried to introduce different 3d metals (e.g., Mn^{2+} , Fe^{2+} , Co^{2+} , and Ni^{2+}) into the action to obtain different novel compounds. However, we failed to obtain any other 3d-metal-containing crystalline PONb products. This may be ascribed to the following two aspects. For one thing, Cu^{2+} ions is an amphoteric cation which can remain stable in both acidic and basic conditions. For another, the $[\text{Cu}(\text{en})_2]^{2+}$ complexes can be regarded as charge compensation cations to effectively balance the high negative charges of the polyoxoniobate. Additionally, the ratio of Cu-organoamine is instrumental in compensating for the high negative charges and adjusting the pH of the reaction system. (2) The organic ligand 1H-1, 2, 3-triazole and pyrrole are indispensable for adjusting the pH when Cu-organoamine is fully chelated, despite their absence in the component of 1 and 2. (3) $\text{K}_2\text{B}_4\text{O}_7\cdot 4\text{H}_2\text{O}$ is an important additive which can not only adjust the pH but also act as mineralizers, which facilitates the crystallization of PONbs; (4) When designing the experiment, we had intended to introduce the main-group metal Tin in the hope to get the heterometallic PONbs. However, using various Tin salts (including SnCl_2 , SnCl_4 , $\text{Sn}(\text{CH}_3)_2\text{Cl}_2$ and $\text{Sn}(\text{CH}_3)_3\text{Cl}$) turned out to be futile in helping us to get the heterometallic PONbs. But at the same time, these Tin salts are essential because without them, our compounds 1 and 2 can not be obtained.

4. Proton conduction experiments: AC impedance measurements were performed on Zennium/IM6 impedance analyzer over the frequency ranging from 0.1 Hz to 10 MHz with an applied voltage of 10 mV. The relative humidity was controlled by a STIKCorp CIHI-150BS3 incubator. The samples were pressed to form a cylindrical pellet of crystalline powder sample (~1 mm thickness \times 5mm diameter) coated with C-pressed electrodes. Two silver electrodes were attached to both sides of the pellet to form four end terminals (quasi-four-probe method). The bulk conductivity was estimated by semicircle fittings of Nyquist plots. The proton conductivity was decided by AC impedance measurements. The σ values of the pellet samples of 1 and 2 were deduced with the operation of a "fit cycle" from the Debye semicircle in the Nyquist plot. The activation energy (E_a) was evaluated using the Arrhenius equation $\sigma T = \sigma_0 \exp(E_a/K_b T)$ and determined by the linear regression analysis.

5. Durability test of 1 and 2 for proton conductivity: After first proton conductivity test, the pellet samples of 1 and 2 were

used again under different relative humidity at 25 °C for three times.

6. Adsorption analysis: Water vapor adsorption were performed at 298K on a micromeritics 3flex Adsorption Analyzer. Samples **1** and **2** were activated by degassed under high vacuum at 313K for 12h to obtain the evacuated samples.

7. Durability test of 1 and 2 for water vapor adsorption: After first water adsorption test, samples of **1** and **2** were activated and degassed under high vacuum at 313K for 12h to remove the water vapor molecule for three cyclic tests.

8. The relationship between relative humidity (RH) and the vapor pressure (P): The relative humidity was controlled by a STIKCorp CIHI-150BS3 incubator, and the corresponding vapour pressure was calculated by RH referencing a CRC handbook.⁵¹

$$P = (RH/100) \times P_0$$

Section S2: Additional Tables

Table S1 Crystallographic data of 1 and 2

	1	2
Empirical formula	C ₂₄ H ₉₆ Cu ₆ N ₂₄ Nb ₆₈ O ₂₀₄	C ₄₀ H ₁₆₀ Cu ₁₀ N ₄₀ Nb ₆₈ O ₂₀₈
Formula weight	10571.59	10892.71
Crystal system	Cubic	Monoclinic
Space group	<i>Pn</i> ³ <i>n</i>	<i>C2/m</i>
<i>a</i> (Å)	43.7163(5)	39.726(3)
<i>b</i> (Å)	43.7163(5)	29.335(2)
<i>c</i> (Å)	43.7163(5)	20.4270(14)
α	90	90
β	90	90.690(2)
γ	90	90
<i>V</i> (Å ³)	83547(3)	23803(3)
<i>Z</i>	8	2
<i>F</i> (000)	40016	10844
Temperature (K)	175(2)	175(2)
μ (mm ⁻¹)	2.146	2.063
Reflns Collected / unique	159830 / 10002	171335 / 17543
restraints / Parameters	12 / 491	186 / 834
Completeness	99.4%	99.9%
GOF on <i>F</i> ²	1.059	1.003
Final <i>R</i> indices (<i>I</i> = 2 σ (<i>I</i>))	<i>R</i> ₁ = 0.0721, <i>wR</i> ₂ = 0.1601	<i>R</i> ₁ = 0.0596, <i>wR</i> ₂ = 0.1695
<i>R</i> indices (all data)	<i>R</i> ₁ = 0.0959, <i>wR</i> ₂ = 0.1719	<i>R</i> ₁ = 0.0758, <i>wR</i> ₂ = 0.1778

$$R_1^a = \sum ||F_o| - |F_c|| / \sum |F_o| \cdot wR_2 = [\sum w(F_o^2 - F_c^2)^2 / \sum w(F_o^2)]^{1/2}$$

Table S2 A summary of known vapor adsorption capacity of POMs materials

Compounds	Amount(cm ³ g ⁻¹)	ref
1	172	This work
2	140	This work
[Cu(en) ₂] ₆ {[Cu(en) ₂] ₆ @[Cu ₂ (trz) ₂ (en) ₂][H ₁₀ Nb ₆₈ O ₁₈₈]}	224	S2
H ₂₀ Cu(en)[Cu(en) ₂] ₁₁ {[Cu(en) ₂] ₆ @[Cu ₂ (en) ₂ (trz) ₂] ₆ (Nb ₆₈ O ₁₈₈)}[4-Tzp] ₂ ·22en·130H ₂ O	219	S3
[Mo ^V ₁₈₀ Mo ^{VI} ₆₀ (OH) ₆₀ O _{620-x} (SO ₃) _{20-x} (SO ₄) _x] ^(80-2x) ·guest	212	S4
[Cu(en) ₂ (H ₂ O)] ₂ {[Cu(en) ₄][Cu(en) ₂] ₅ {[Cu(en) ₂ KNb ₂₄ O ₇₂ H ₁₀] ₂ ·6en·70H ₂ O	204	S5
K ₄ @[Cu ₂₉ (OH) ₇ (H ₂ O) ₂ (en) ₈ (trz) ₂₁][Nb ₂₄ O ₆₇ (OH) ₂ (H ₂ O) ₃] ₄	193	S2
[Cu(en) ₂] ₆ @[Cu ₂ (en) ₂ (trz) ₂] ₆ (Nb ₆₈ O ₁₈₈)	188	S2
[Zn ₁₂ (trz) ₂₀][SiW ₁₂ O ₄₀] ₁₁ ·H ₂ O	150	S6
K ₃ [Cr ₃ O(OOCH) ₆ (H ₂ O) ₃][R-SiW ₁₂ O ₄₀]	130	S7
Cu ₆ (Trz) ₁₀ (H ₂ O) ₄ [H ₂ SiW ₁₂ O ₄₀] ₈ ·8H ₂ O	118	S8
[Cu ₄ (dpdo) ₁₂][H(H ₂ O) ₂₇ (CH ₃ CN) ₁₂][PW ₁₂ O ₄₀] ₃	65.1	S9
K ₂ [Cr ₃ O(OOCH) ₆ (mepy) ₃] ₂ [α -PMo ₁₂ O ₄₀] ₃ ·5H ₂ O	56.8	S10
H ₁₄ [Na ₆ (H ₂ O) ₁₂] ₄ [K ₄₂ Ge ₈ W ₇₂ O ₂₇₂ (H ₂ O) ₆₀] ₁ ·solvent	52	S11
[Cu ₃ (L) ₂ (H ₂ O) ₄][Cu(dmf) ₄ (SiW ₁₂ O ₄₀)]·9H ₂ O	51.7	S12

H[Ni(Hbpdcc)(H ₂ O) ₂] ₂ [PW ₁₂ O ₄₀] ₂ ·8H ₂ O }	31	S13
[Co(pn) ₃] ₄ [PNb ₁₂ O ₄₀ (VO) ₆][OH] ₅ ·20H ₂ O	19.72	S14
(DODA) ₂₃ [Mo ₁₅₄ O ₄₆₂ H ₅] ₂ ·70H ₂ O	16.6	S15
Cs _{3.6} K _{0.4} [PW ₁₁ O ₃₉ (Sn-OH)]·8H ₂ O	0.31	S16
K ₂ [Cr ₃ O(OOCH) ₆ (mepy) ₃] ₂ [a-SiW ₁₂ O ₄₀]·2H ₂ O·CH ₃ OH	0.03	S17
Cs ₂ [Cr ₃ O(OOCC ₂ H ₅) ₆ (H ₂ O) ₃] ₂ [R-SiW ₁₂ O ₄₀]·4H ₂ O	0.022	S18, S19
Cs ₃ H _{0.3} [SiW ₁₂ O ₄₀] _{0.83} ·3H ₂ O	0.020	S20

[a] Trz: 1,2,4-triazole; dpdo: 4,4'-bipyridine-N,N'-dioxide; mepy: 4-methylpyridine; L: N,N-bis[(2-hydroxy-3-methoxyphenyl)methylidene] hydrazine hydrate; dmf: N,N-Dimethylformamide; H₂bpdcc : 2,2'-bipyridyl-3,3'-dicarboxylic acid ; pn: 1,2-diaminopropane ; DODA: dimethyldioctadecylammonium.

Table S3 The calculation of the activation energy (E_a) of 1

T/K	1000/T	R/Ω	$\sigma/S\text{ cm}^{-1}$	lnσT	slope	E_a
298.15 (25 °C)	3.35	6141.60	1.24×10^{-4}	-3.29	-12.241	$E_{a1} = 1.04\text{ eV}$
308.15 (35 °C)	3.24	1351.52	5.65×10^{-4}	-1.75		
318.15 (45 °C)	3.14	498.41	1.53×10^{-3}	-0.72		
318.15 (45 °C)	3.14	498.41	1.53×10^{-3}	-0.72	-4.789	$E_{a1}' = 0.41\text{ eV}$
328.15 (55 °C)	3.05	302.27	2.53×10^{-3}	-0.18		
338.15 (65 °C)	2.96	218.36	3.50×10^{-3}	0.16		
348.15 (75 °C)	2.87	145.47	5.25×10^{-3}	0.60		

Table S4 The calculation of the activation energy (E_a) of 2

T/K	1000/T	R/Ω	$\sigma/S\text{ cm}^{-1}$	lnσT	slope	E_a
298.15 (25 °C)	3.35	7897.60	9.68×10^{-5}	-3.55	-12.001	$E_{a2} = 1.02\text{ eV}$
308.15 (35 °C)	3.24	2358.30	3.24×10^{-4}	-2.30		
318.15 (45 °C)	3.14	670.12	1.14×10^{-3}	-1.01		
318.15 (45 °C)	3.14	670.12	1.14×10^{-3}	-1.01	-6.285	$E_{a2}' = 0.53\text{ eV}$
328.15 (55 °C)	3.05	328.72	2.32×10^{-3}	-0.27		
338.15 (65 °C)	2.96	195.13	3.91×10^{-3}	0.28		
348.15 (75 °C)	2.87	133.73	5.71×10^{-3}	0.69		

Section 3: Additional structural figures and characterizations

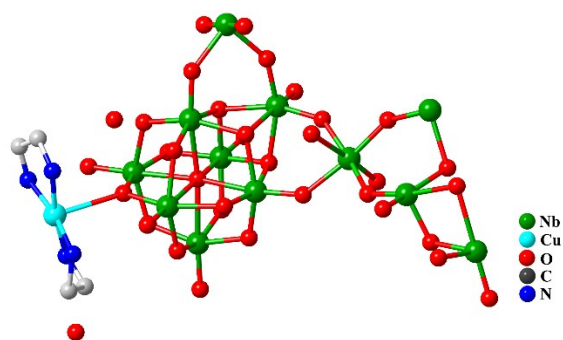


Fig. S1 The asymmetric unit of **1**.

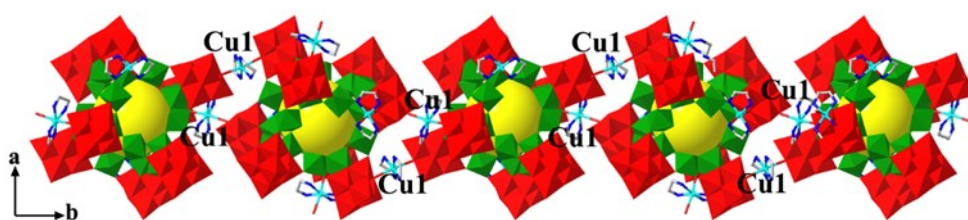


Fig. S2 1D chain structure in compound **1** along the *c* axis.

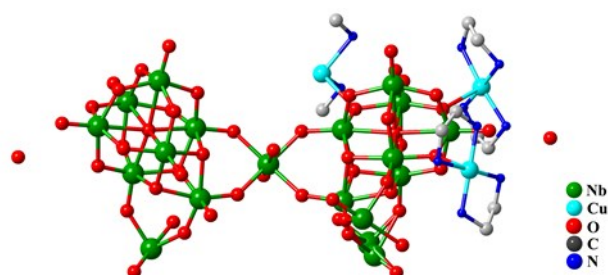


Fig. S3 The asymmetric unit of **2**.

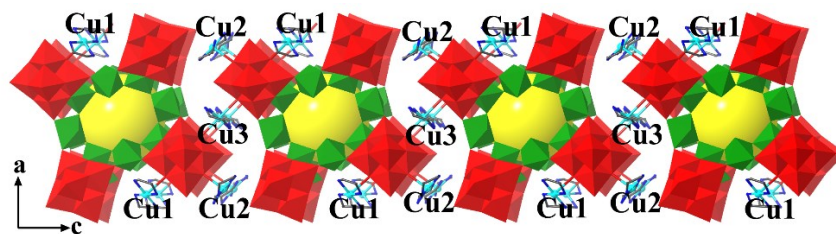


Fig. S4 1D chain structure in compound **2** along the *b* axis.

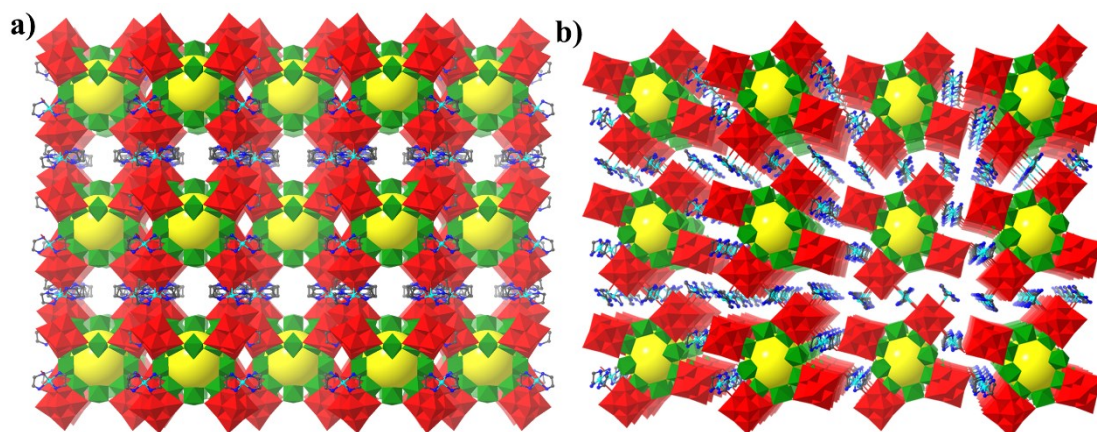


Fig. S5 3D frameworks in **2** along the *a* axis and *b* axis

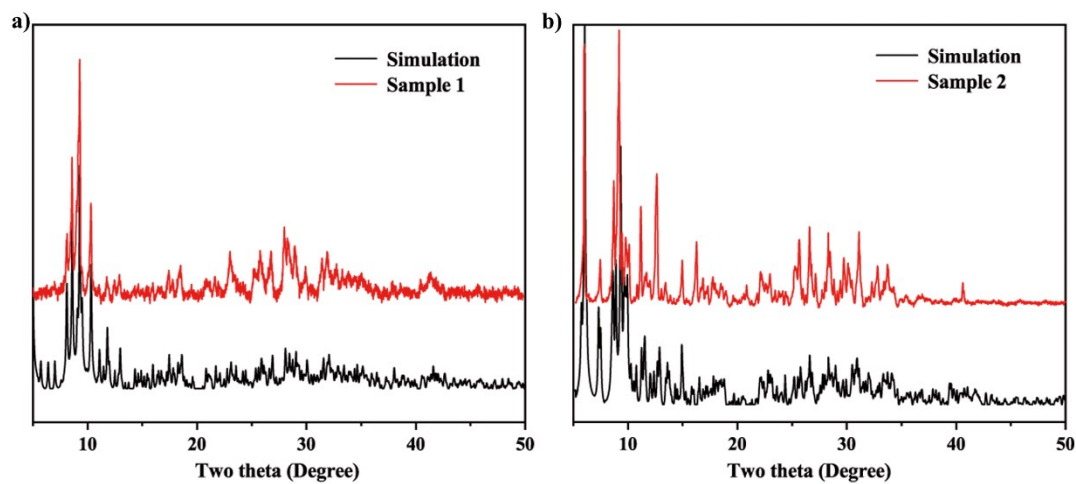


Fig. S6 Simulated and experimental PXRD patterns of **1** and **2**.

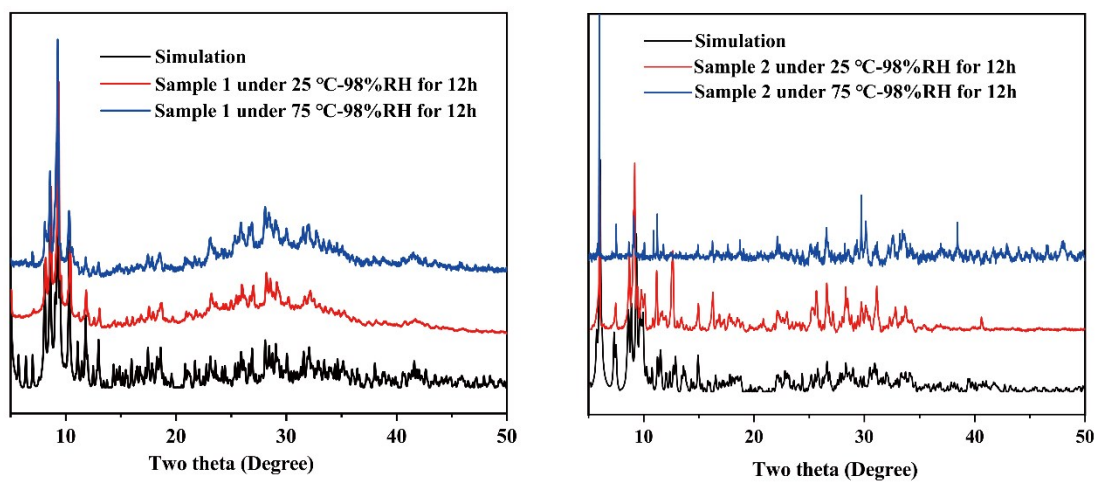


Fig. S7 PXRD patterns of the as-synthesized sample **1** and **2** under variable-temperature at 98% RH

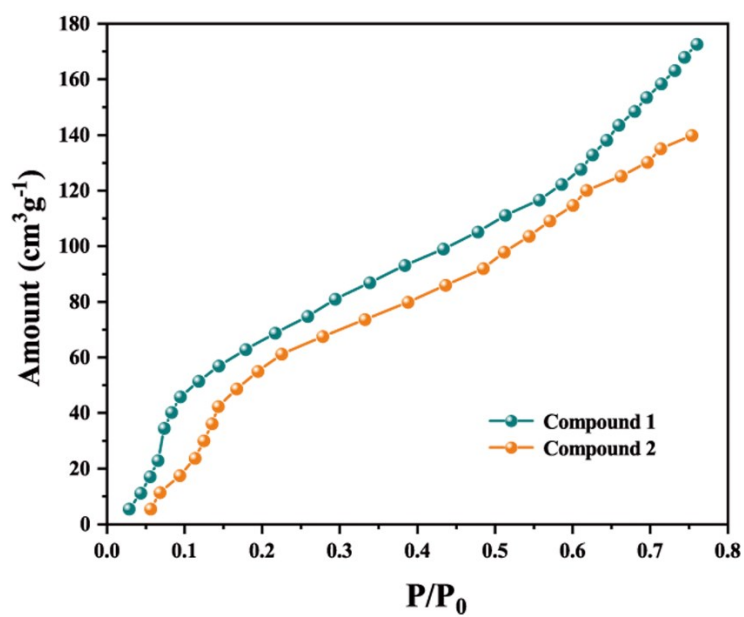


Fig. S8 Water adsorption isotherms of 1 and 2.

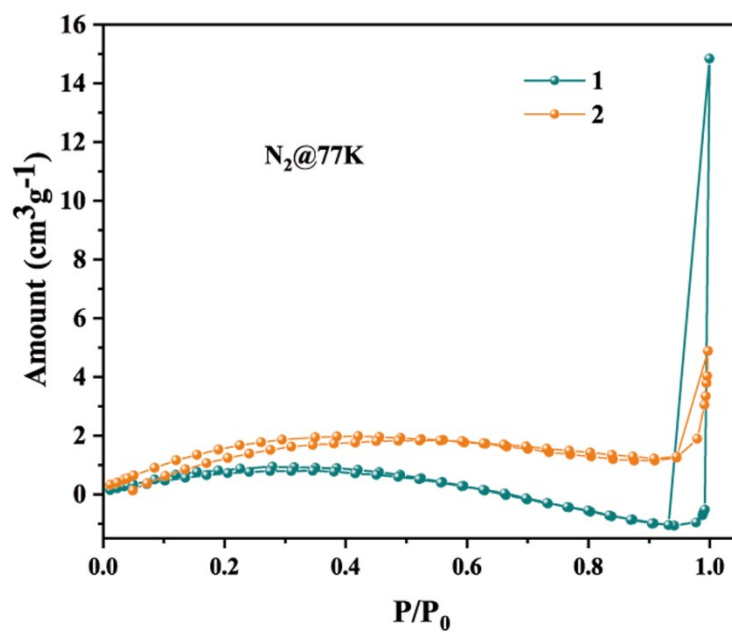


Fig. S9 N_2 adsorption isotherms of 1 and 2.

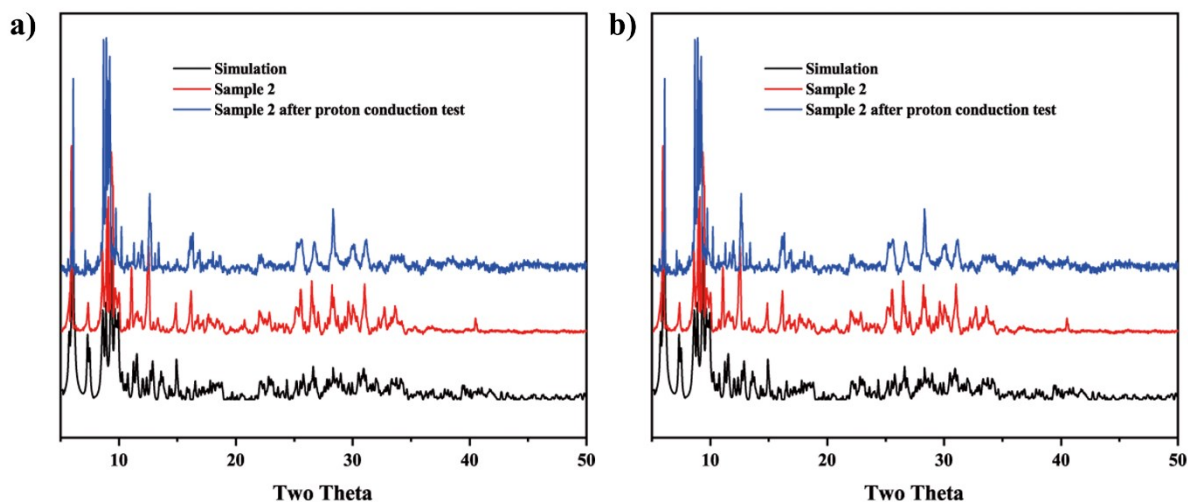


Fig. S10 PXRD patterns of 1 and 2 after proton conduction test.

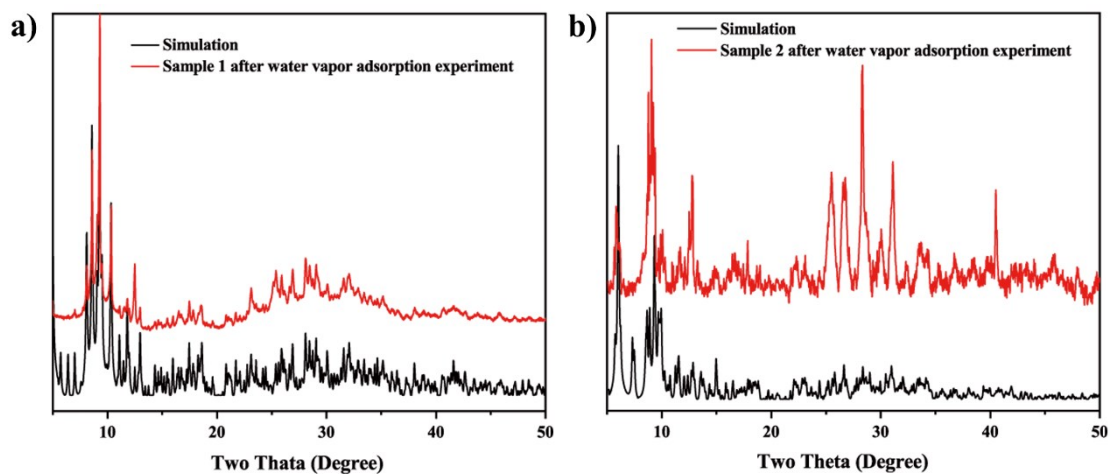


Fig. S11 PXRD patterns of 1 and 2 after water vapor adsorption test.

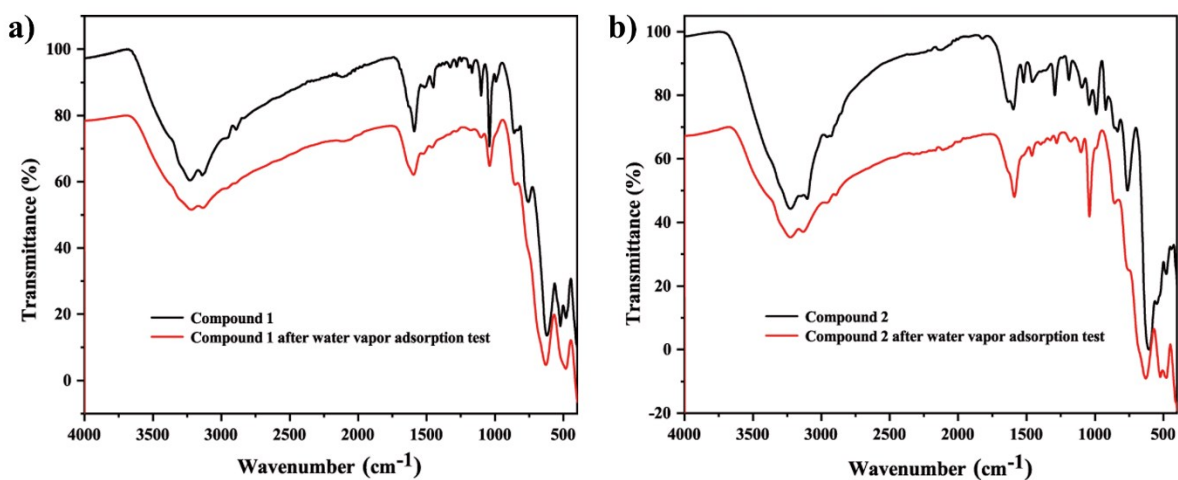


Fig. S12 IR spectra of samples 1 a) and 2 b) after water vapor adsorption test.

In the IR spectra, the broad absorption peak at 3230 cm^{-1} is attributed to the $\nu(\text{O-H})$ stretching vibration of water. The $\nu(\text{C-H})$ and $\nu(\text{N-H})$ stretching vibrations appear at about 3140 cm^{-1} and 2930 cm^{-1} and their bending vibrations adsorption appear at about 1100 cm^{-1} and 1600 cm^{-1} . The absorption peak at about 1040 cm^{-1} is attributed to the stretching vibration peak of Cu-O. The peaks that appear in the range of 400 to 1000 cm^{-1} can be attributed to the characteristic absorption peak of Nb-O, of which 854 cm^{-1} is the stretching vibration peak of $\nu(\text{Nb-O}_t)$ and 620 cm^{-1} and 475 cm^{-1} are the stretching vibration peaks of $\nu(\text{Nb-O}_b\text{-Nb})$.

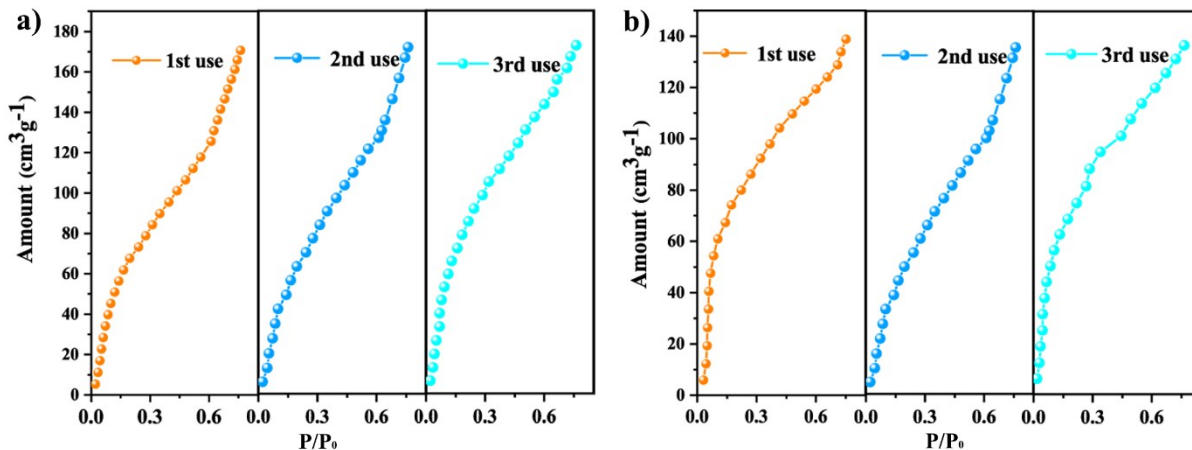


Fig. S13. Water adsorption isotherms of **1** a) and **2** b) for three cycles, respectively.

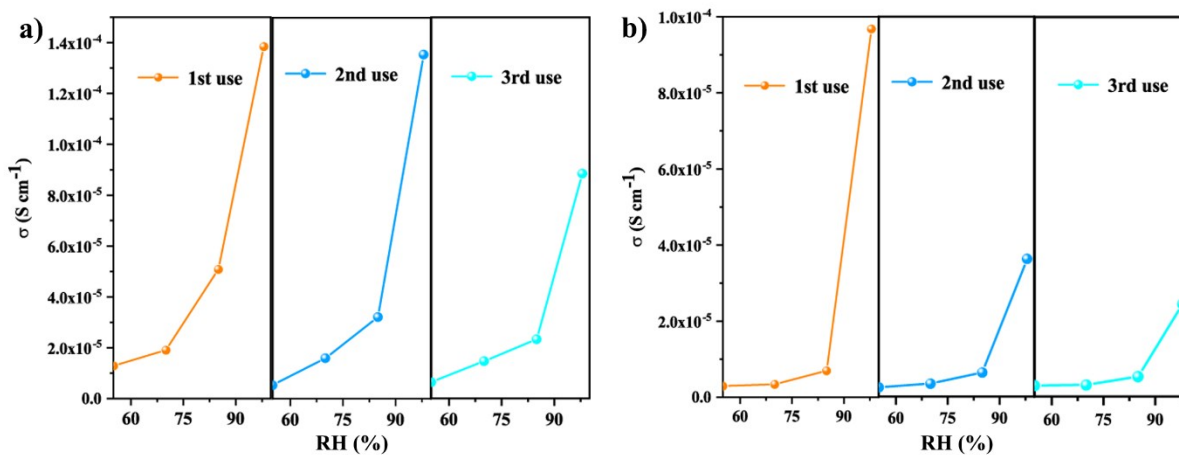


Fig. S14. Proton conductivity of **1** a) and **2** b) as a function of relative humidity at $25\text{ }^{\circ}\text{C}$ for three cycles, respectively.

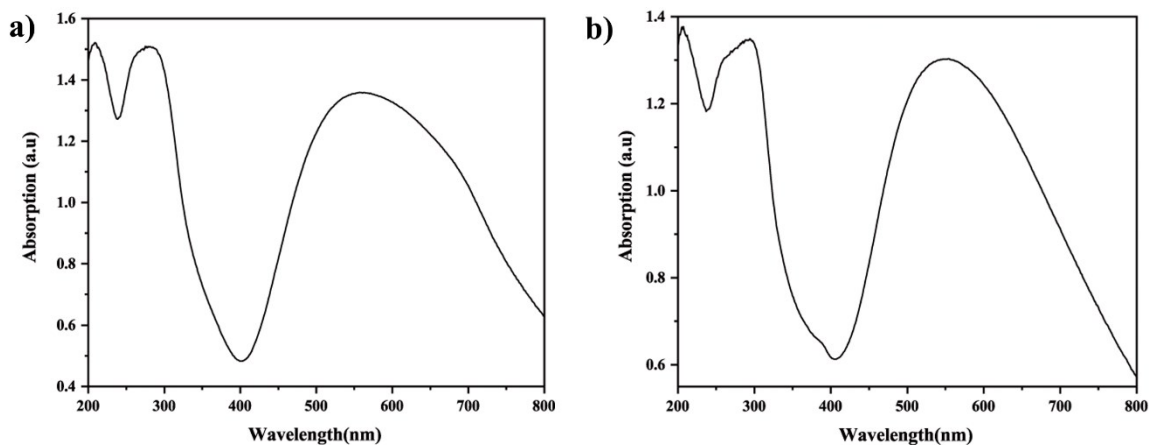


Fig. S15. The solid-state diffuse reflectance UV-vis spectra of samples **1** and **2**.

The UV diffuse spectra of two compounds are determined to be in the range of 200 to 800 nm. The absorption peak in the range of 200 to 400 nm can be attributed to the charge transfer transitions from O to Nb. The broad absorption peak in the range of 400 to 800 nm can be attributed to the d-d transition of the 3d metal ion Cu^{2+} .

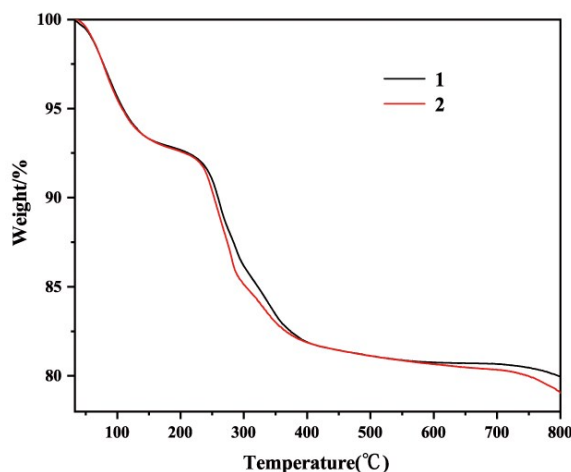


Fig. S16. TG curves of samples **1** and **2**.

The thermogravimetric curves of compounds **1** and **2** were measured at a heating rate of 10 °C/min in an argon atmosphere, and the temperature range of the test was from 30 °C to 800 °C. As shown in Fig. S16, compound **1** and **2** has a continuous weight loss process in the temperature range of 30 °C to 800 °C. The first weight-loss stage that occurs when the temperature was within the range of 30 °C to 250 °C should be ascribed to the loss of lattice water molecules. Based on the first weight-loss of about 14% for **1** and **2**, there are about 52 and 54 lattice water molecules, respectively.

Section S4: References

- S1 A. Wexler, CRC Handbook of Chemistry and Physics, W. M. Haynes, CRC Press, Taylor & Francis Group Boca Raton London New York, 97th edition, 2016-2017, Section 15: PRACTICAL LABORATORY DATA, Constant Humidity Solution, 15-31.
- S2 Z. K. Zhu, Y. Y. Lin, H. Yu, X. X. Li, S. T. Zheng, *Angew. Chem. Int. Ed.*, 2019, **58**, 16864.
- S3 Z. K. Zhu, Y. Y. Lin, L.D. Lin, X. X. Li, Y. Q. Sun and S. T. Zheng, *Inorg. Chem.*, 2020, **59**, 11925.
- S4 J. M Lin, N, Li, S. P. Yang, M. J. Jia, J. Liu, X. M. Li, L. An, Q. W. Tian, L. Z. Dong, Y. Q. Lan, *J. Am. Chem. Soc.*, 2020, **142**, 13982.
- S5 Z. K. Zhu, L.D. Lin, J. Zhang, X. X. Li, Y. Q. Sun and S. T. Zheng, *Inorg. Chem. Front.*, 2020, **7**, 3919.
- S6 E. L. Zhou, C. Qin, X. L. Wang, K. Z. Shao and Z. M. Su, *Chem. Eur. J.*, 2015, **21**, 13058.
- S7 S. Uchida, R. Kawamoto, N. Mizuno, *Inorg. Chem.*, 2006, **45**, 5136.
- S8 E. L. Zhou, C. Qin, P. Huang, X. L. Wang, W. C. Chen, K. Z. Shao and Z. M. Su, *Chem. Eur. J.*, 2015, **21**, 11894.
- S9 M. Wei.; L. Chen, X. Duan, *J. Coord. Chem.*, 2014, **67**, 2809.
- S10 R. Kawahara, S. Uchida, N. Mizuno, *Chem. Mater.*, 2015, **27**, 2092.
- S11 Z. Li, L. D. Lin, H. Yu, X. X. Li and S. T. Zheng, *Angew. Chem. Int. Ed.*, 2018, **57**, 15777.
- S12 M. L. Wei.; J. J. Sun, X. Y. Duan, *Eur. J. Inorg. Chem.*, 2014, 345.
- S13 M. L. Wei, X. X. Wang, J. J. Sun and X. Y. Duan, *J. Solid. State. Chem.*, 2013, **202**, 200.
- S14 J. F. Hu, Y. Q. Xu, D. K. Zhang, B. K. Chen, Z.G. Lin and C.W. Hu, *Inorg. Chem.*, 2017, **56**, 10844.
- S15 S. Noro, R. Tsunashima, Y. Kamiya, K. Uemura, H. Kita, L. Cronin, T. Akutagawa, T. Nakamura, *Angew. Chem. Int. Ed.*, 2009,

48, 8703.

S16 Y. K. Miura, H. Imai, T. Yokoi, T. Tatum, Y. Kamiya, *Microporous Mesoporous Mater.*, 2013, **174**, 34.

S17 S. Uchida, R. Eguchi, N. Mizuno, *Angew. Chem. Int. Ed.*, 2010, **49**, 9930.

S18 A. Lesbani, R. Kawamoto, S. Uchida, N. Mizuno, *Inorg. Chem.*, 2008, **47**, 3349.

S19 C. J. Jiang, A. Lesbani, R. Kawamoto, S. Uchida, N. Mizuno, *J. Am. Chem. Soc.*, 2006, **128**, 14240.

S20 Y. Ogasawara, S. Uchida, T. Maruichi, R. Ishikawa, N. Shibata, Y. Ikuhara, N. Mizuno, *Chem. Mater.*, 2013, **25**, 905.